CLEO CONF 97-29
EPS97 393

Observation of Two Narrow States Decaying Into $\Xi_c^+\gamma$ and $\Xi_c^0\gamma$

CLEO Collaboration

(August 15, 1997)

Abstract

Using 5 fb^{-1} of data recorded by the CLEO II detector at CESR in the energy region around 10.5 GeV, we report the preliminary observation of two narrow states in the decay modes $\Xi_c^+\gamma$ and $\Xi_c^0\gamma$. We observe 25 ± 6 and 28 ± 7 events respectively. The Ξ_c^+ has been detected in the decay modes $\Xi^-\pi^+\pi^+$ and $\Xi^0\pi^+\pi^0$, and the Ξ_c^0 has been detected in the decay modes $\Xi^-\pi^+$, $\Xi^-\pi^+\pi^0$, $\Xi^0\pi^+\pi^-$, and Ω^-K^+. We interpret the observed signals as the $\Xi_c'(c\{sq\})$, the partners of the already-established charmed strange baryon Ξ_c $(c[sq])$, where $\{sq\}$ denotes symmetry with respect to the exchange of light quarks and $[sq]$ denotes antisymmetry. The preliminary mass differences M($\Xi_c^{+\prime}$)-M(Ξ_c^+) and M($\Xi_c^{0\prime}$)-M(Ξ_c^0) have been measured to be $107.8 \pm 1.7 \pm 2.5$ MeV/c^2 and $107.0 \pm 1.4 \pm 2.5$ MeV/c^2, respectively.

T. E. Coan,[1] V. Fadeyev,[1] I. Korolkov,[1] Y. Maravin,[1] I. Narsky,[1] V. Shelkov,[1] J. Staeck,[1] R. Stroynowski,[1] I. Volobouev,[1] J. Ye,[1] M. Artuso,[2] A. Efimov,[2] M. Goldberg,[2] D. He,[2] S. Kopp,[2] G. C. Moneti,[2] R. Mountain,[2] S. Schuh,[2] T. Skwarnicki,[2] S. Stone,[2] G. Viehhauser,[2] X. Xing,[2] J. Bartelt,[3] S. E. Csorna,[3] V. Jain,[3,*] K. W. McLean,[3] S. Marka,[3] R. Godang,[4] K. Kinoshita,[4] I. C. Lai,[4] P. Pomianowski,[4] S. Schrenk,[4] G. Bonvicini,[5] D. Cinabro,[5] R. Greene,[5] L. P. Perera,[5] G. J. Zhou,[5] B. Barish,[6] M. Chadha,[6] S. Chan,[6] G. Eigen,[6] J. S. Miller,[6] C. O'Grady,[6] M. Schmidtler,[6] J. Urheim,[6] A. J. Weinstein,[6] F. Würthwein,[6] D. W. Bliss,[7] G. Masek,[7] H. P. Paar,[7] S. Prell,[7] M. Sivertz,[7] V. Sharma,[7] D. M. Asner,[8] J. Gronberg,[8] T. S. Hill,[8] D. J. Lange,[8] S. Menary,[8] R. J. Morrison,[8] H. N. Nelson,[8] T. K. Nelson,[8] C. Qiao,[8] J. D. Richman,[8] D. Roberts,[8] A. Ryd,[8] M. S. Witherell,[8] R. Balest,[9] B. H. Behrens,[9] W. T. Ford,[9] H. Park,[9] J. Roy,[9] J. G. Smith,[9] J. P. Alexander,[10] C. Bebek,[10] B. E. Berger,[10] K. Berkelman,[10] K. Bloom,[10] D. G. Cassel,[10] H. A. Cho,[10] D. S. Crowcroft,[10] M. Dickson,[10] P. S. Drell,[10] K. M. Ecklund,[10] R. Ehrlich,[10] A. D. Foland,[10] P. Gaidarev,[10] R. S. Galik,[10] L. Gibbons,[10] B. Gittelman,[10] S. W. Gray,[10] D. L. Hartill,[10] B. K. Heltsley,[10] P. I. Hopman,[10] J. Kandaswamy,[10] P. C. Kim,[10] D. L. Kreinick,[10] T. Lee,[10] Y. Liu,[10] G. S. Ludwig,[10] N. B. Mistry,[10] C. R. Ng,[10] E. Nordberg,[10] M. Ogg,[10,†] J. R. Patterson,[10] D. Peterson,[10] D. Riley,[10] A. Soffer,[10] B. Valant-Spaight,[10] C. Ward,[10] M. Athanas,[11] P. Avery,[11] C. D. Jones,[11] M. Lohner,[11] C. Prescott,[11] J. Yelton,[11] J. Zheng,[11] G. Brandenburg,[12] R. A. Briere,[12] A. Ershov,[12] Y. S. Gao,[12] D. Y.-J. Kim,[12] R. Wilson,[12] H. Yamamoto,[12] T. E. Browder,[13] Y. Li,[13] J. L. Rodriguez,[13] T. Bergfeld,[14] B. I. Eisenstein,[14] J. Ernst,[14] G. E. Gladding,[14] G. D. Gollin,[14] R. M. Hans,[14] E. Johnson,[14] I. Karliner,[14] M. A. Marsh,[14] M. Palmer,[14] M. Selen,[14] J. J. Thaler,[14] K. W. Edwards,[15] A. Bellerive,[16] R. Janicek,[16] D. B. MacFarlane,[16] P. M. Patel,[16] A. J. Sadoff,[17] R. Ammar,[18] P. Baringer,[18] A. Bean,[18] D. Besson,[18] D. Coppage,[18] C. Darling,[18] R. Davis,[18] N. Hancock,[18] S. Kotov,[18] I. Kravchenko,[18] N. Kwak,[18] S. Anderson,[19] Y. Kubota,[19] S. J. Lee,[19] J. J. O'Neill,[19] S. Patton,[19] R. Poling,[19] T. Riehle,[19] V. Savinov,[19] A. Smith,[19] M. S. Alam,[20] S. B. Athar,[20] Z. Ling,[20] A. H. Mahmood,[20] H. Severini,[20] S. Timm,[20] F. Wappler,[20] A. Anastassov,[21] J. E. Duboscq,[21] D. Fujino,[21,‡] K. K. Gan,[21] T. Hart,[21] K. Honscheid,[21] H. Kagan,[21] R. Kass,[21] J. Lee,[21] M. B. Spencer,[21] M. Sung,[21] A. Undrus,[21,§] R. Wanke,[21] A. Wolf,[21] M. M. Zoeller,[21] B. Nemati,[22] S. J. Richichi,[22] W. R. Ross,[22] P. Skubic,[22] M. Bishai,[23] J. Fast,[23] J. W. Hinson,[23] N. Menon,[23] D. H. Miller,[23] E. I. Shibata,[23] I. P. J. Shipsey,[23] M. Yurko,[23] S. Glenn,[24] S. D. Johnson,[24] Y. Kwon,[24,**] S. Roberts,[24] E. H. Thorndike,[24] C. P. Jessop,[25] K. Lingel,[25] H. Marsiske,[25] M. L. Perl,[25] D. Ugolini,[25]

[*]Permanent address: Brookhaven National Laboratory, Upton, NY 11973.

[†]Permanent address: University of Texas, Austin TX 78712

[‡]Permanent address: Lawrence Livermore National Laboratory, Livermore, CA 94551.

[§]Permanent address: BINP, RU-630090 Novosibirsk, Russia.

[**]Permanent address: Yonsei University, Seoul 120-749, Korea.

R. Wang,[25] and X. Zhou[25]

[1]Southern Methodist University, Dallas, Texas 75275
[2]Syracuse University, Syracuse, New York 13244
[3]Vanderbilt University, Nashville, Tennessee 37235
[4]Virginia Polytechnic Institute and State University, Blacksburg, Virginia 24061
[5]Wayne State University, Detroit, Michigan 48202
[6]California Institute of Technology, Pasadena, California 91125
[7]University of California, San Diego, La Jolla, California 92093
[8]University of California, Santa Barbara, California 93106
[9]University of Colorado, Boulder, Colorado 80309-0390
[10]Cornell University, Ithaca, New York 14853
[11]University of Florida, Gainesville, Florida 32611
[12]Harvard University, Cambridge, Massachusetts 02138
[13]University of Hawaii at Manoa, Honolulu, Hawaii 96822
[14]University of Illinois, Champaign-Urbana, Illinois 61801
[15]Carleton University, Ottawa, Ontario, Canada K1S 5B6
and the Institute of Particle Physics, Canada
[16]McGill University, Montréal, Québec, Canada H3A 2T8
and the Institute of Particle Physics, Canada
[17]Ithaca College, Ithaca, New York 14850
[18]University of Kansas, Lawrence, Kansas 66045
[19]University of Minnesota, Minneapolis, Minnesota 55455
[20]State University of New York at Albany, Albany, New York 12222
[21]Ohio State University, Columbus, Ohio 43210
[22]University of Oklahoma, Norman, Oklahoma 73019
[23]Purdue University, West Lafayette, Indiana 47907
[24]University of Rochester, Rochester, New York 14627
[25]Stanford Linear Accelerator Center, Stanford University, Stanford, California 94309

I. INTRODUCTION

CLEO [1,2] and other experimental groups [3–6] have previously reported the observation of the $J^P = \frac{1}{2}^+$ Ξ_c^0 (c[sd]) and Ξ_c^+ (c[su]) baryons, where [su] and [sd] denote the antisymmetric nature of the wave functions with respect to interchange of the light quarks. Recently, CLEO announced the observation of both the $J^P = \frac{3}{2}^+$ Ξ_c^{*0} [7] and the Ξ_c^{*+} [8] states. CLEO II has already reconstructed several hundred events of both the Ξ_c^+ and Ξ_c^0 [7–9]. The partners of the above charmed strange baryons are the $\Xi_c^{+\prime}$ (c{su}) and $\Xi_c^{0\prime}$ (c{sd}), where {su} and {sd} specify the wave functions are symmetric with respect to interchange of the light quarks. In this report we present the first preliminary evidence for the $\Xi_c^{+\prime}$ and $\Xi_c^{0\prime}$ states.

Ground state charmed strange baryons (csq, $q = u$ or d) have $l = 0$ and $l^{'} = 0$, where l is the quantum number that corresponds to the orbital angular momentum between the light quarks, $l^{'}$ corresponds to the angular momentum between the heavy charm quark and the light diquark pair. The two light quarks, q and s may be assumed to form a diquark of spin 0 or 1. The spin 0 state can then combine with the spin $\frac{1}{2}$ c-quark to form the $J^P = \frac{1}{2}^+$ antisymmetric doublet, represented by the Ξ_c states. The spin 1 diquark state can combine with the spin $\frac{1}{2}$ c-quark to give the symmetric $J^P = \frac{1}{2}^+$ $\Xi_c^{\prime}$ and $J^P = \frac{3}{2}^+$ Ξ_c^* doublets. The Ξ_c^*, $\Xi_c^{\prime}$, and Ξ_c states belong to the $\mathbf{6}^*$, $\mathbf{6}$, and $\overline{\mathbf{3}}$ representations of SU(3) within the $J^P = \frac{3}{2}^+$ SU(4) 20-plet and $J^P = \frac{1}{2}^+$ SU(4) 20-plet, respectively. CLEO has also recently reported the first evidence for an excited charmed strange baryon beyond the SU(4) 20-plets, the Ξ_{c1}^+ [10], thought to be the $J^P = \frac{3}{2}^-$, $l^{'} = 1$ charmed strange analogue of the $\Lambda_{c1}^+(2625)$.

Since the Ξ_c and $\Xi_c^{\prime}$ have the same J^P and charge, they are expected to mix. According to some authors [11,12] the mixing is small so that the Ξ_c is mostly antisymmetric and the $\Xi_c^{\prime}$ mostly symmetric. There are several theoretical models that predict the mass splitting M($\Xi_c^{+\prime}$) - M(Ξ_c^+) to be in the range 100 - 114 MeV/c^2 [11–26]. According to these theoretical estimates for the M($\Xi_c^{\prime}$) - M(Ξ_c) mass splitting, the only allowed decay is the radiative decay $\Xi_c^{\prime} \to \Xi_c\gamma$. According to most authors the $\Xi_c^{\prime}$ state should be below the π threshold for the decay into $\Xi_c\pi$. However, the Ξ_c^*'s are expected to be heavy enough to decay according to $\Xi_c^* \to \Xi_c\pi$. These theoretical models also predict the mass difference M(Ξ_c^*) - M($\Xi_c^{\prime}$) to be about 60-70 MeV/c^2.

II. DATA SAMPLE

The data sample used in this analysis corresponds to an integrated luminosity of 4.96 fb^{-1} from the $\Upsilon(4S)$ energy region and energies just below the $\Upsilon(4S)$ resonance (around 10.5 GeV), collected with the CLEO II detector [27] operating at CESR. Charmed baryons can be produced from either secondary decays of B mesons or directly from e^+e^- annihilations into $c\overline{c}$ jets. In this analysis, we have used x_p and $x_p^{\prime}$ to refer to the scaled momentum of the Ξ_c^+ and $\Xi_c^{+\prime}$, respectively. These are defined as $x_p^{'} = p^{'}/p_{max}^{'}$ and $x_p = p/p_{max}$, where $p_{max}^{'} = \sqrt{E_{beam}^2 - m_{\Xi_c^{+\prime}}^2}$ and $p_{max} = \sqrt{E_{beam}^2 - m_{\Xi_c^+}^2}$ with E_{beam} equal to the beam energy. We limit our search to $x_p^{\prime} > 0.5$ to avoid the combinatorial background which dominates at low $x_p^{\prime}$. This requirement also eliminates charm baryons from B meson decay.

III. THE CLEO II DETECTOR

We will describe briefly the parts of the detector relevant to this analysis. The CLEO II detector is designed to detect both charged and neutral particles with excellent resolution and efficiency. The detector consists of a charged particle tracking system surrounded by a scintillation counter based time-of-flight system and an electromagnetic calorimeter consisting of 7800 thallium-doped cesium iodide crystals. The tracking system, time-of-flight scintillators and calorimeter are installed inside a 1.5 T superconducting solenoidal magnet. The momentum resolution of the tracking system is given by $(\delta p/p)^2 = (0.15p\%)^2 + (0.5\%)^2$, where p is the track momentum in GeV/c. Charge measurements from the drift chamber wires provide specific ionization loss (dE/dx) information. The photon energy resolution achieved by the electromagnetic calorimeter [28] varies from 4.2% at 100 MeV to 1.4% at 5 GeV.

Identification of hadrons is achieved by using dE/dx measurements and time-of-flight (TOF) if available. By itself, the dE/dx measurement provides two standard deviation (σ) π/K separation up to 0.7 GeV/c. Time-of-flight measurements extend the 2 σ π/K separation up to 1.1 GeV/c and 2 σ p/K separation up to 1.7 GeV/c. The dE/dx and TOF measurements are combined to define a joint $\chi^2_i = [\{(dE/dx)_{\rm measured} - (dE/dx)_{\rm expected}\}/\sigma_{dE/dx}]^2_i + [\{(T)_{\rm measured} - (T)_{\rm expected}\}/\sigma_{\rm TOF}]^2_i$, where i corresponds to the pion, kaon, and proton hypotheses. A χ^2-probability is then calculated for each hypothesis. A charged track is defined to be consistent with a pion (proton) hypothesis, if its probability to be a pion (proton) is greater than 0.001.

IV. ANALYSIS PROCEDURE

The vertex of the Ξ_c' decay in CLEO II is indistinguishable from its production point at the event vertex. We reconstruct Ξ_c' by combining hyperons Λ, Ξ^0, Ξ^-, and Ω^-, that have well-separated secondary vertices, with tracks from the primary event vertex to make Ξ_c candidates, then add a photon to make Ξ_c'. Good secondary vertices are characterized by the distance of the hyperon decay vertex from the event vertex in the $r-\phi$ plane (greater than 2 mm for Λ and Ξ^-, 3 mm for Ξ^0), the difference in z positions of the two tracks forming the vertex (less than 2 cm for Λ, Ξ^0, and Ω^-, 2.5 cm for Ξ^-), and reconstructed hyperon trajectories that do point back to the primary event vertex, in the case of Ξ^-, Ξ^0, and Ω^-. Charge conjugation is implied throughout this analysis.

A. Λ Reconstruction

Candidates for $\Lambda \to p\pi^-$ are reconstructed from two oppositely charged tracks, assuming the higher momentum one to be a proton and requiring it to be consistent with the proton particle identification hypothesis. The invariant mass of the combination is calculated using a three-dimensional vertex-constrained fit at the point of intersection. $p\pi^-$ combinations within 5 MeV/c^2 of the nominal Λ mass are accepted as Λ candidates. We recalculate the four momentum vectors of the Λ candidates using a kinematic fit to the nominal mass of the Λ. With these Λ we later reconstruct Ξ^-, Ω^- and Ξ^0 candidates.

B. Ξ^- Reconstruction

The Ξ^- candidates are formed by combining each Λ candidate with the remaining negatively charged tracks in the event consistent with a pion hypothesis. We reconstruct Ξ^- candidates by finding the intersection between Λ and π^- and performing a three-dimensional vertex-constrained fit, requiring the Λ and π^- to come from a common vertex. We require that the π^- point away from the primary event vertex. Figure 1(a) shows the invariant mass distribution for $\Lambda\pi$ combinations. A Gaussian fit to this distribution yields a total of 11578 ± 125 reconstructed Ξ^- candidates. All $\Lambda\pi^-$ combinations within 5 MeV/c^2 of the nominal Ξ^- mass are accepted as Ξ^- candidates. The 4-momentum of the Ξ^- candidate is recalculated by performing a kinematic fit to the mass of Ξ^-.

C. Ω^- Reconstruction

For Ω^- reconstruction, we combine each Λ candidate with each remaining negatively charged particle in the event, assuming it to be a kaon. We require the K^- candidates to have P($\chi^2 > 0.01$) for the kaon hypothesis. Using a process similar to Ξ^- reconstruction, we reconstruct Ω^- first by finding the intersection of Λ and K^- in the $r - \phi$ plane and performing a three-dimensional vertex-constraint fit requiring the Λ and K^- to come from a common vertex. We require the kaon to not point back to the primary event vertex. Since the Ω^- has a very short lifetime we do not require any cut on the radial distance of Ω^- from the event vertex. The invariant mass distribution for all ΛK^- combinations is shown in Figure 1(b). The fit shows a total of 373 ± 32 events in the signal. All ΛK^- combinations within 5 MeV/c^2 of the fitted Ω^- mass are defined as Ω^- candidates. The 4-momentum of the candidate is recalculated by performing a kinematic fit to the mass of the Ω^-.

D. Ξ^0 Reconstruction

The Ξ^0 candidates are reconstructed from Λ and π^0 pairs. The candidates for π^0 are formed from a pair of photons with at least one photon satisfying the barrel requirement of $|\cos\theta| < 0.707$, where θ is the angle between the photon and the beam line. We select showers consistent with photons based on the ratio of the energy of the nine crystals closest to the shower center to that of the twenty-five closest crystals (E9/E25 contour cut). We require the energy of photons to be greater than 50 MeV and exclude showers that match charged tracks projected into the calorimeter. The $\gamma\gamma$ combinations for π^0 candidates are kinematically fitted to the π^0 mass hypothesis, with origin at the Ξ^0 vertex, and we require the χ^2 of the fit to be less than 10. In Figure 1(c) the invariant mass distribution for $\Lambda\pi^0$ combinations is plotted, yielding 7568 ± 227 for the fitted signal area. $\Lambda\pi^0$ combinations within 8 MeV/c^2 of the fit are defined as Ξ^0 candidates. The 4-momentum vector of the candidate is recalculated by performing a kinematic fit to the mass of Ξ^0.

E. Ξ_c^+ Reconstruction

We now proceed to search for Ξ_c^+ in two modes, $\Xi_c^+ \to \Xi^-\pi^+\pi^+$ and $\Xi_c^+ \to \Xi^0\pi^+\pi^0$. For Ξ_c reconstruction, we select good tracks from the primary event vertex by requiring the miss distance in the $r-\phi$ plane to be less than 2 mm and the z coordinate at the closest point to the primary vertex to be less than 3.5 cm. We reject tracks with poor measurement resolution. We require the tracks to be consistent with the pion particle identification hypothesis. For the $\Xi^-\pi^+\pi^+$ channel we require the π^+ momentum to be greater than 100 MeV/c. To suppress background in the $\Xi^0\pi^+\pi^0$ channel, we require both the π^+ and the π^0 to have a momentum greater than 250 MeV/c. The invariant mass combinations of $\Xi^-\pi^+\pi^+$ with $x_p > 0.5$ are plotted in Figure 2 (a). We fit the distribution to a Gaussian function with a width of 8.0 MeV/c^2 as predicted by Monte Carlo plus a low-order polynomial background and obtain a yield of 154.8 $\pm$ 15.0 events. For $\Xi_c^+ \to \Xi^0\pi^+\pi^0$, mass plots for $x_p > 0.6$ are shown in Figure 2 (b). A fit to a Gaussian function with width fixed at the Monte Carlo prediction of 15.0 MeV/c^2 yields 70.2 $\pm$ 13.6 events.

Combinations with invariant mass within 2.0 σ of the Ξ_c^+ mass are defined as Ξ_c^+ candidates. Based on the Ξ_c^+ widths for the three modes, 2.0 σ falls within 17 MeV/c^2 for the $\Xi^-\pi^+\ \pi^+$ channel and 30 MeV/c^2 for the $\Xi^0\pi^+\pi^0$ channel.

F. $\Xi_c^{+\prime}$ Reconstruction

To reconstruct $\Xi_c^{+\prime}$, Ξ_c^+ candidates as defined in the last section are combined with photons of energy greater than 100 MeV. We use only showers that are detected in the barrel CsI crystals, $|cos(\theta)| < 0.707$, where θ is the angle between the photon and the beam line. Any showers matched to charged tracks projected into the calorimeter are excluded. We select showers consistent with photons based on the ratio of the energy of the nine crystals closest to the shower center. These photons are also required to satisfy the E9/E25 contour cut, which accepts 99% of good photons. Poorly reconstructed showers are rejected. Photons which form part of a good $\pi^0 \to \gamma\gamma$ are not used in the $\Xi_c^+\gamma$ combinations, since we require an isolated photon candidate. Good π^0 candidates are selected as described above in the Ξ^0 reconstruction section.

Instead of the invariant mass distribution for $\Xi_c^+\gamma$, we plot the mass difference $\Delta M = M(\Xi_c^+\gamma) - M(\Xi_c^+)$, where $M(X)$ refers to the reconstructed mass of the X candidate. The errors associated with the reconstruction of the Ξ_c^+ tend to cancel out in the difference, so that we achieve better mass resolution in the mass difference distribution. We now relax any cut on the x_p of the Ξ_c^+, but do require that x_p' of the $\Xi_c^+\gamma$ combinations be greater than 0.5 for $\Xi^-\pi^+\pi^+$, and greater than 0.6 for $\Xi^0\pi^+\pi^0$.

In Figure 4 (a) and (b), we show the $\Xi_c^+\gamma$ invariant mass difference distributions corresponding to the $\Xi^-\pi^+\pi^+$ and $\Xi^0\pi^+\pi^0$ decays of Ξ_c^+, respectively. To get the signal area, we fit the distribution to the sum of a smooth first-order polynomial and a Gaussian function with width fixed at the Monte Carlo prediction of about 5 MeV/c^2. We obtain 16.1$\pm$5.1 events in $\Xi^-\pi^+\pi^+$ and 7.5$\pm$3.6 in $\Xi^0\pi^+\pi^0$. $\Delta M = 108$ MeV/c^2 corresponding to the $\Xi^-\pi^+\pi^+$ decay mode. When the signals in the two Ξ_c^+ modes are added, we get Figure 5 (a) which shows a clear enhancement at $\Delta M = (107.8 \pm 1.7)$ MeV/c^2. Fitting this distribution yields a signal area of 25 ± 6 events, which has a statistical significance of 4.2 σ.

We have repeated the analysis, keeping all the selection criteria the same as before, except that we drop the π^0 veto requirement. When the π^0 veto requirement is not made, there is a significant background from $\Xi_c^{*+} \to \Xi_c^+ \pi^0$. We include a contribution for this background, as modeled by Monte Carlo, in the fit. We also use a threshold function to model the background going to zero at low mass difference. Figure 5 (b) shows the combined mass distribution without the π^0 veto requirement. The signal size increases from 25.5 ± 6.5 to 32.0 ± 10.6 events, consistent with the Monte Carlo prediction.

G. Ξ_c^0 Reconstruction

The first two channels for Ξ_c^0 reconstruction involve Ξ^-, namely $\Xi_c^0 \to \Xi^- \pi^+$ and $\Xi^- \pi^+ \pi^0$. Charged pions used above are required to be consistent with the pion hypothesis. Each photon pair ($\gamma\gamma$) combination within 12.5 MeV/c^2 (2.5 σ) of the nominal π^0 mass is used as a π^0 candidate. The momentum is recalculated by fitting to the mass of π^0 and only fits with χ^2 less than 10 are accepted. In Figures 3(a) and (b), we show the invariant mass distributions for all $\Xi^- \pi^+$ and $\Xi^- \pi^+ \pi^0$ combination with x_p greater than 0.5.

For the third Ξ_c^0 decay mode, all combinations of $\Omega^- K^+$ pairs are formed. Only charged tracks consistent with the kaon hypothesis are used. Figure 3(c) shows the invariant mass plot for $\Omega^- K^+$ combinations with $x_p > 0.5$.

The fourth decay mode for reconstructing Ξ_c^0 is $\Xi^0 \pi^+ \pi^-$. Here also, we reject tracks that are not consistent with the pion hypothesis. Figure 3(d) shows the invariant mass distribution for $\Xi^0 \pi^+ \pi^-$ combinations with a tighter cut of $x_p > 0.6$ used to further reduce the background.

In Figures 3(a), (b), (c) and (d), in each case we also show fits to the data distribution with the sum of a Gaussian signal with width fixed at the Monte Carlo predicted values and a smooth polynomial background. The results of these fits yield 133$\pm$41, 86$\pm$13, 24$\pm$5, and 46$\pm$10 events corresponding to Ξ_c^0 decays to the above four modes, respectively. We select combinations having an invariant mass within two standard deviations of the nominal Ξ_c^0 mass for use as Ξ_c^0 candidates.

H. $\Xi_c^{0\prime}$ Reconstruction

Once the Ξ_c^0 has been reconstructed, we plot the mass difference $M(\Xi_c^0 \gamma) - M(\Xi_c^0)$, instead of the invariant mass of $\Xi_c^0 \gamma$ combination, since the mass difference is measured with better resolution due to common errors canceling out. We select photon candidates as described above in the $\Xi_c^{+\prime}$ reconstruction. To further reduce the combinatorial background we require the x_p' of the $\Xi_c^{0\prime}$ to be greater than 0.5. We do not make any explicit cut on x_p of Ξ_c^0.

In Figures 6(a), (b), (c) and (d), we show the invariant mass difference distributions for M($\Xi_c^0 \gamma$) - M(Ξ_c^0), corresponding to $\Xi^- \pi^+ \gamma$, $\Xi^- \pi^+ \pi^0 \gamma$, $\Omega^- K^+ \gamma$, and $\Xi^0 \pi^+ \pi^- \gamma$, respectively. These distributions are fit with the sum of a Gaussian signal shape with a fixed Monte Carlo width of approximately 5 MeV/c^2, and a low-order polynomial background. We obtain 7.0 ± 4.0, 11.6 ± 4.4, 3.8 ± 2.0, and 6.0 ± 3.3 events for the four decay modes, respectively.

There is a clear enhancement around ΔM = 108 MeV/c^2 in the distribution corresponding to $\Xi_c^0 \to \Xi^- \pi^+ \pi^0$. The other Ξ_c^0 decay modes contribute supporting fluctuations in the same mass region so that the sum of the four mass distributions gives a statistically significant enhancement, as shown in Figure 7 (a). This fit yields 28.0 ± 7.1 events at a mass difference of 107.0$\pm$1.4 MeV/c^2. We repeat the above analysis, keeping all selection criteria the same, except we do not reject photons which are also reconstructed as π^0 candidates. Figure 7(b) is the combined distribution plot with no π^0 veto. We obtain 45.5 ± 10.0 events, consistent with the predictions of the Monte Carlo simulation of the veto efficiency.

V. RESULTS AND CONCLUSIONS

For our final result, we use the mass differences found in the analyses with the π^0 veto, because the mass is measured more accurately in the case with less background in both cases. We studied the effects of various background shapes, variation of cuts, and the calibration of our mass difference scale using $D_s^* \to D_s \gamma$ decays. The only difference we found was the variation in the background shape due to relaxing the π^0 veto, which in turn causes a upward shift in the mass difference. We assign a preliminary systematic error of 2.5 MeV/c^2 based on this variation to both mass differences.

In conclusion, we have observed two narrow resonances decaying to $\Xi_c^+ \gamma$ and $\Xi_c^0 \gamma$. The preliminary results for the mass differences M($\Xi_c^{+\prime}$)-M(Ξ_c^+) and M($\Xi_c^{0\prime}$)-M(Ξ_c^0) are measured to be $107.8 \pm 1.7 \pm 2.5$ MeV/c^2 and $107.0 \pm 1.4 \pm 2.5$ MeV/c^2, respectively. This is in good agreement with the theoretical expectations for these mass differences. Since the $J^P = \frac{3}{2}^+$ charmed strange baryons Ξ_c^{*+} and Ξ_c^{*0} have already been observed by CLEO, the best interpretation of the observed resonances in $\Xi_c^+ \gamma$ and $\Xi_c^0 \gamma$ would be as the $J^P = \frac{1}{2}^+$ $\Xi_c^{+\prime}$ and $\Xi_c^{0\prime}$, respectively.

ACKNOWLEDGMENTS

We gratefully acknowledge the effort of the CESR staff in providing us with excellent luminosity and running conditions. This work was supported by the National Science Foundation, the U.S. Department of Energy, the Heisenberg Foundation, the Alexander von Humboldt Stiftung, Research Corporation, the Natural Sciences and Engineering Research Council of Canada, and the A.P. Sloan Foundation.

REFERENCES

[1] M. S. Alam *et al.* Phys. Lett. **B226**, 401 (1989).
[2] P. Avery *et al.* Phys. Rev. Lett. **62**, 863 (1989).
[3] S. Biagi *et al.* Phys. Lett. **B150**, 230 (1985)
S. Biagi *et al.* Z. Phys. **C28**, 175, (1985).
[4] P. Coteus *et al.* Phys. Rev. Lett. **59**, 1530 (1987).
[5] S. Barlag *et al.* Phys. Lett. **B236**, 495 (1990).
[6] H. Albrecht *et al.* Phys. Lett. **B247**, 121 (1990).
[7] P. Avery *et al.* Phys. Rev. Lett. **75**, 4364-4368 (1995).
[8] L. Gibbons *et al.* Phys. Rev. Lett. **77**, 810-813 (1996).
[9] K. Edwards *et al.* Phys. Lett. **B373**, 362 (1996).
[10] G. Brandenburg *et al.* EPS97-398, CLEO CONF 97-17 (This conference) (1997).
[11] J. Franklin, Phys Rev. **D53**, 564-565 (1996).
[12] C. Glenn Boyd, M. Lu, and M. J. Savage, Phys Rev. **D55**, 5474 (1997).
[13] R. E. Cutkosky and P. Geiger, Phys. Rev **D48**, 1315 (1993).
[14] T. Ito *et al.* Z. Phys. **C59** 57-62 (1993).
[15] J. G. Körner, M. Krämer and D. Pirjol, Prog. Part. Nucl. Physics **33**, 787-868 (1994).
[16] R. Roncaglia, D. B. Lichtenberg, and E. Predazzi, Phys. Rev. **D52**, 1722 (1995).
[17] M. J. Savage, Phys. Lett. **B359**, 189-193, (1995).
[18] A. Falk, Phys. Rev. Lett **77**, 223-226 (1996).
[19] R. Lebed, Phys Rev. **D54**, 4463-4473 (1996).
[20] E. Jenkins, Phys. Rev. **D54**, 4515-4531 (1996).
[21] UKQCD Collaboration (K. C. Bowler *et al.*), Phys. Rev. **D54** 3619-3633 (1996).
[22] J. Dey *et al.* Phys. Lett. **B375**, 358 (1996).
[23] D. B. Lichtenberg *et al.* Phys. Rev. **D53**, 6678 (1996).
[24] W. S. Carvalho and A. C. B. Antunes, hep-ph/9404298 (1994).
[25] L. Burakovsky *et al.* hep-ph/9706464 (1997).
[26] A. Zalewska and K. Zalewski, hep-ph/9608240 (1996).
[27] Y. Kubota *et al.* Nucl. Instr. and Meth. **A320**, 66 (1992).
[28] E. Blucher *et al.* Nucl. Instr. and Meth. **A249**, 201 (1989).

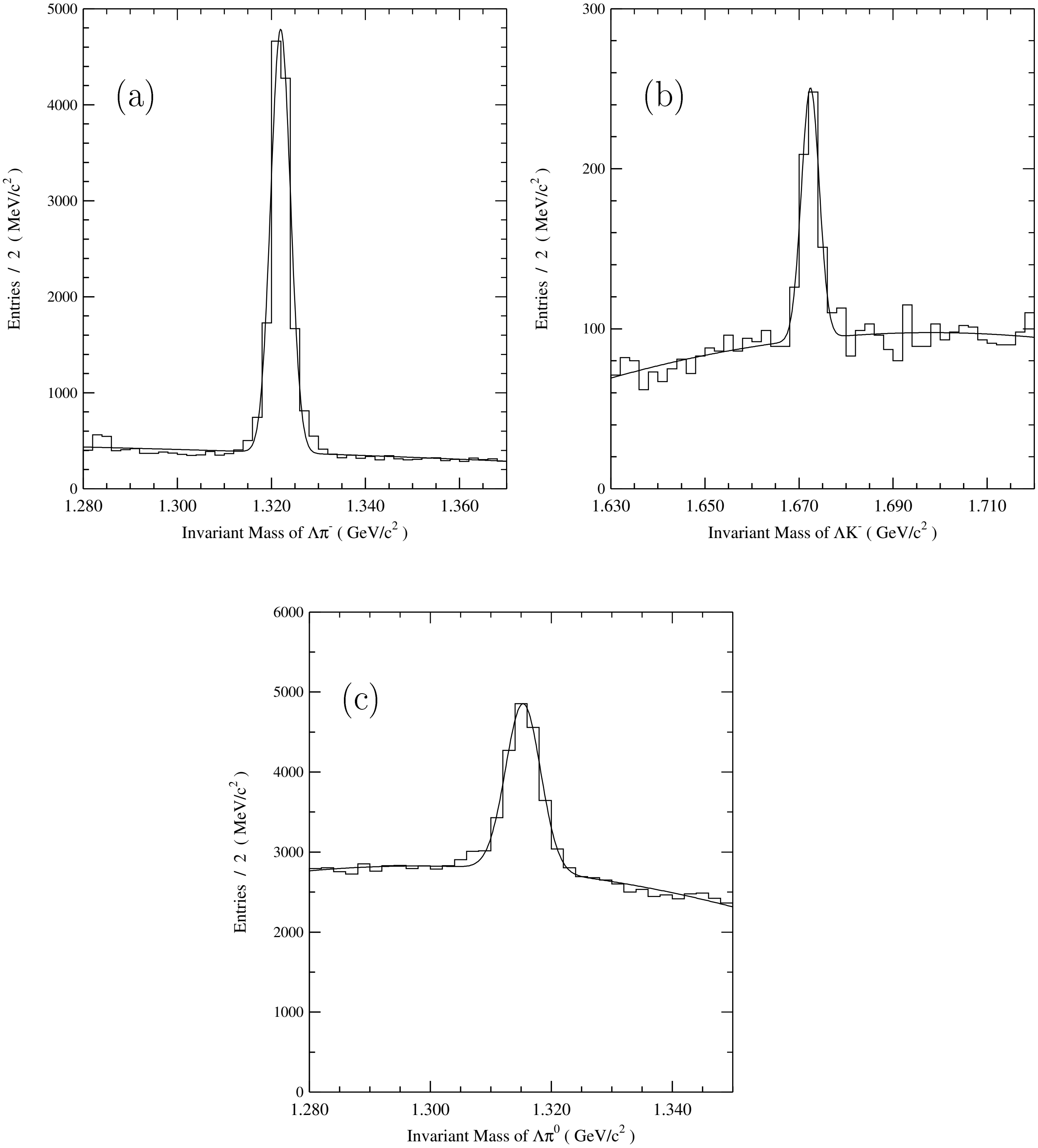

FIG. 1. Invariant mass distribution of (a) $\Xi^-\to\Lambda\pi^-$, (b) $\Omega^-\to\Lambda K^-$ and (c) $\Xi^0\to\Lambda\pi^0$.

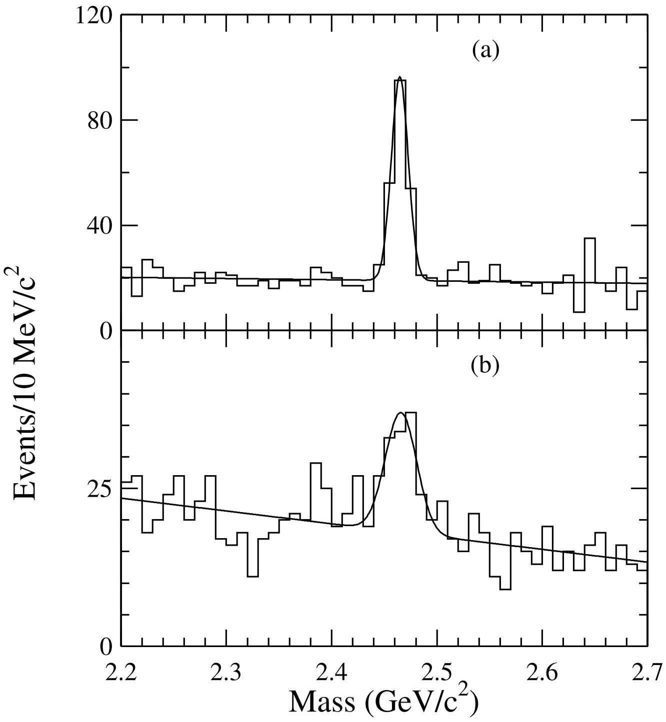

FIG. 2. Invariant mass combinations for (a) $\Xi_c^+ \to \Xi^- \pi^+ \pi^+$(b) $\Xi_c^+ \to \Xi^0 \pi^+ \pi^0$.

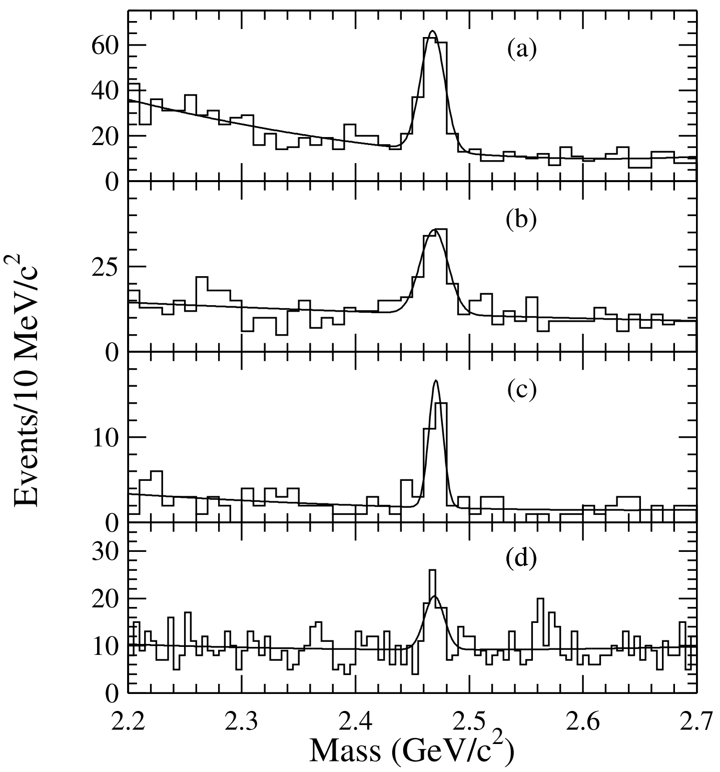

FIG. 3. Invariant mass plots for $\Xi_c^0 \to$ (a) $\Xi^- \pi^+$, (b) $\Xi^- \pi^+ \pi^0$, (c) $\Omega^- K^+$ and (d) $\Xi^0 \pi^+ \pi^-$.

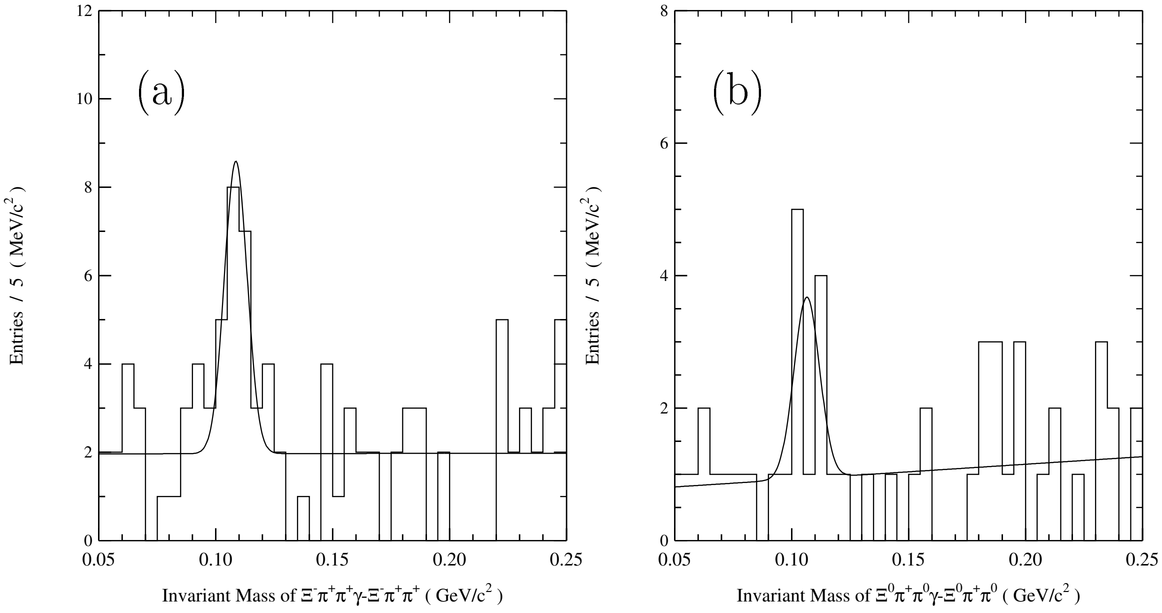

FIG. 4. Invariant mass difference $M(\Xi_c^+\gamma) - M(\Xi_c^+)$ with π^0 rejection for (a) $\Xi^-\pi^+\pi^+\gamma$ - $\Xi^-\pi^+\pi^+$, (b) $\Xi^0\pi^+\pi^0\gamma$ - $\Xi^0\pi^+\pi^0$.

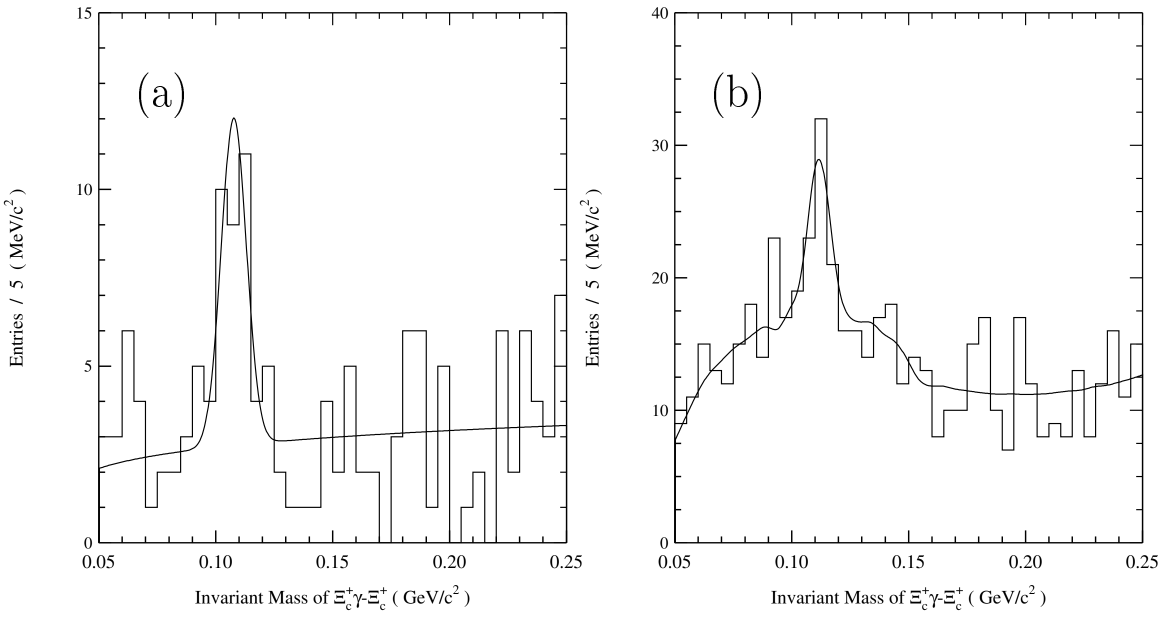

FIG. 5. Combined invariant mass difference of $M(\Xi_c^+\gamma) - M(\Xi_c^+)$. (a) is with π^0 rejection and (b) is without π^0 rejection.

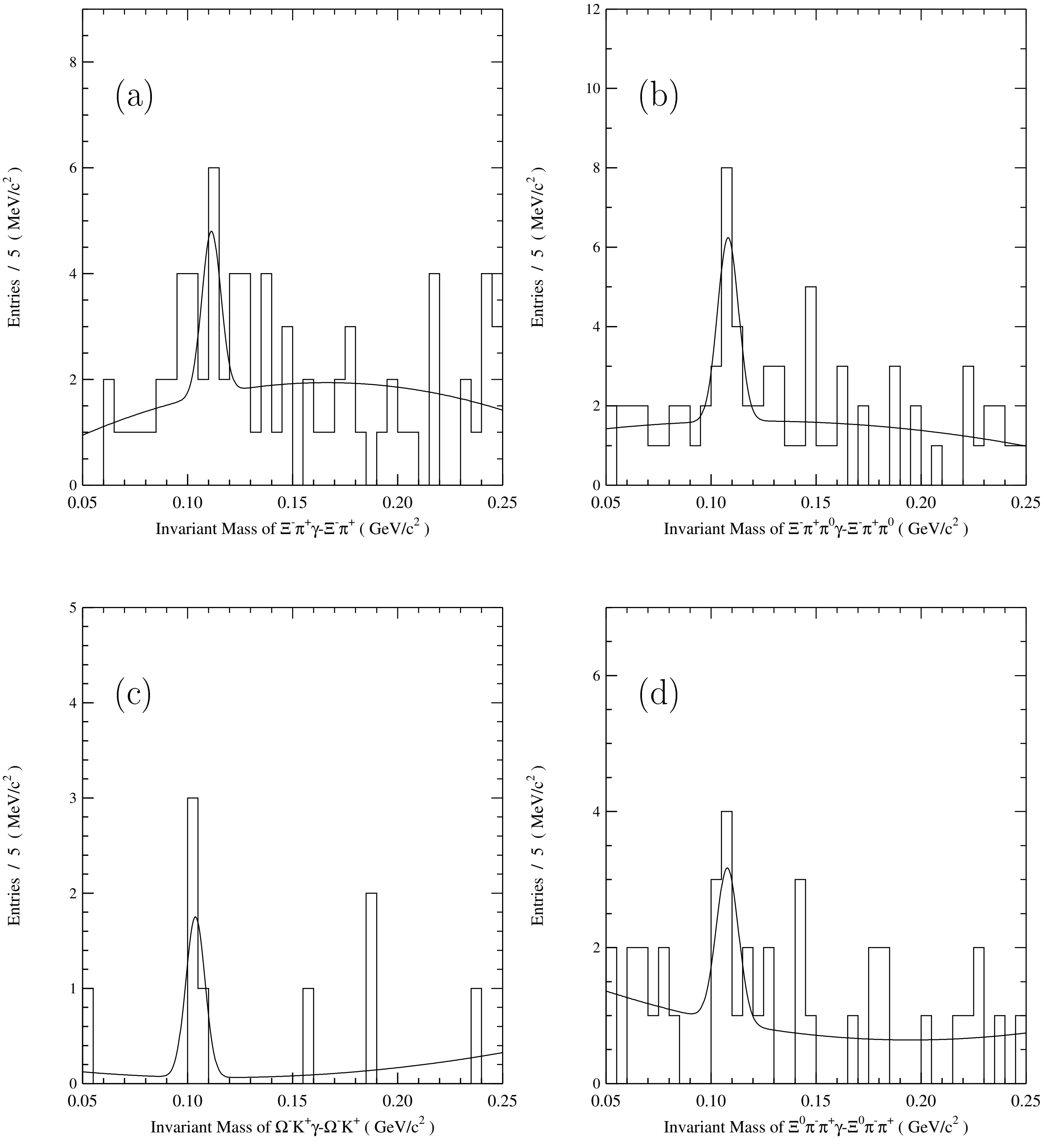

FIG. 6. Invariant mass difference $M(\Xi_c^0\gamma) - M(\Xi_c^0)$ with π^0 rejection for (a) $\Xi^-\pi^+\gamma$ - $\Xi^-\pi^+$, (b) $\Xi^-\pi^+\pi^0\gamma$ - $\Xi^-\pi^+\pi^0$, (c) $\Omega^-K^+\gamma$ - Ω^-K^+ and (d) $\Xi^0\pi^+\pi^-\gamma$ - $\Xi^0\pi^+\pi^-$.

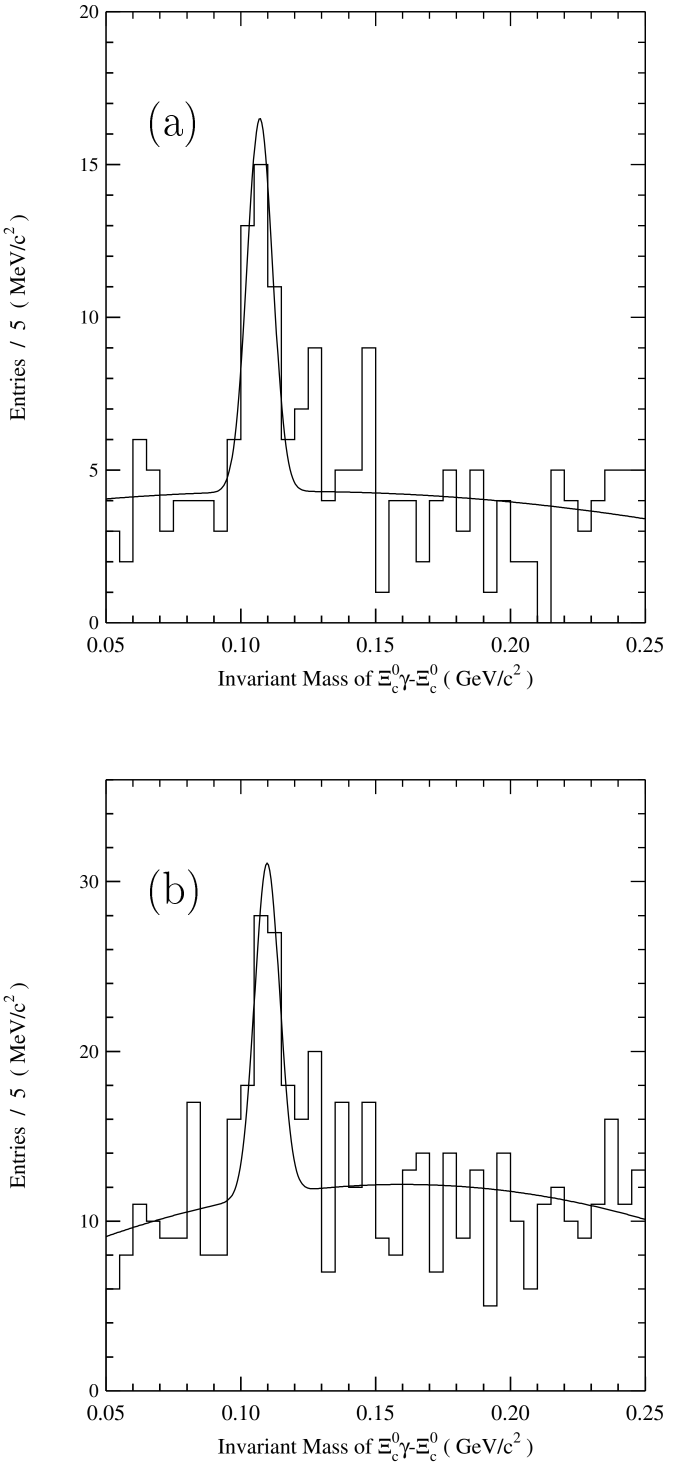

FIG. 7. Combined invariant mass difference of $M(\Xi_c^0\gamma) - M(\Xi_c^0)$. (a) is with π^0 rejection and (b) is without π^0 rejection.